Heliyon 10 (2024) e30405

Contents lists available at ScienceDirect

Heliyon

journal homepage: www.cell.com/heliyon

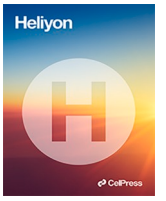

Research article

Defect identification of electricity transmission line insulators based on the improved lightweight network model with computer vision assistance

Chen Lanhang

College of Electrical and Information Engineering, Jiangsu University, Zhenjiang, Jiangsu Province, 212000, China

ARTICLE INFO

Keywords:
Computer vision
Lightweight network
Depth separable convolution
GraphCut segmentation
Electricity transmission line insulator

ABSTRACT

This work aims to ensure the safe operation of electricity transmission lines and reduce costs and maintenance difficulties. It studies the application of computer vision (CV) in the defect identification of electricity transmission lines. In addition, this work proposes a method to improve the lightweight network model to provide an effective identification model to solve the problem of electricity transmission line defects. Firstly, GraphCut segmentation and Laplace algorithms are employed to expand and sharpen the electricity transmission line image. Secondly, in light of the Depth Separable Convolution algorithm, a defect detection model for the electricity transmission line insulator is proposed based on the You Only Look Once 4 (YOLOv4) network. Moreover, MobileNetV1 is utilized to improve this lightweight network model. Finally, this work uses ImageNet, a large public dataset, to validate the proposed model experimentally. The research results reveal that: (1) In the model testing results, all research indicators of the model are greater than 90 %, indicating an excellent detection accuracy of this model. (2) The improved YOLOv4 model can increase the detection speed to 53 frames/s at the cost of 2.4 % accuracy. (3) After image sharpening, the improved YOLOv4 model has promoted the insulator defects' detection ability to a certain extent. The above outcomes suggest that the improved YOLOv4 model can predict more efficiently and accurately and reduce unnecessary false positives. This illustrates that the proposed model is feasible and is expected to be applied to the defect identification of electricity transmission lines in practice. These findings fully demonstrate this work's vital value in enhancing the prediction efficiency and accuracy, thus offering a strong preference for the defect identification of electricity transmission lines in practical applications.

1. Introduction

The transmission equipment inspection mainly includes methods such as manual labor, helicopters, unmanned aerial vehicles (UAVs), robots, and online monitoring. Under special weather and location conditions, it is difficult to detect line faults through manual inspections, and the efficiency of manual inspections is relatively low [1,2]. Helicopter inspection has some problems, such as high resource consumption, high personal risk, high technical requirements, and high altitude control. It can not meet the inspection requirements under various voltage levels, geographical conditions, and special meteorological conditions. Technologies such as UAV inspection, online monitoring, and robot inspection can obtain visible light, infrared, and ultraviolet image data of power transmission

E-mail address: chenlanhang@126.com.

https://doi.org/10.1016/j.heliyon.2024.e30405
Received 11 January 2024; Received in revised form 22 April 2024; Accepted 25 April 2024
Available online 4 May 2024

lines and their auxiliary power components, and perform status detection. They have the advantages of low cost, high efficiency, strong practicality, and flexible operation, and have gradually become an essential means of power inspection. However, the above inspection methods produce a large number of images and videos. Relying only on inspectors for visual judgment can inevitably lead to low efficiency and easy misjudgment. Target detection and image recognition in computer vision (CV) can meet the needs of processing, analyzing, and intelligently detecting many inspection images. They can provide technical means for power grid operation and maintenance personnel to intelligently analyze and identify transmission equipment inspection images [3]. CV technology shows remarkable advantages in transmission equipment inspection. It can efficiently process massive image data, accurately identify fault points, improve inspection efficiency, and reduce misjudgment rate [4]. Compared with traditional inspection methods, CV is more intelligent and efficient, helps to ensure the safe and stable operation of the power grid, and is a crucial assistance for developing the power industry.

Presently, the integration of computer vision (CV) technology for assessing the condition of electricity transmission line structures and their associated components has transitioned into practical application. However, several challenges persist: 1) The model training dataset is unbalanced [5]. Applying deep learning (DL) models to defect detection requires massive labeled image data to train a high-precision and robust detection model. Nevertheless, practical scenarios often lack adequate defect samples to satisfy the training requisites of intelligent detection models. 2) Model reliability diminishes in complex environments. The transmission channel's surroundings exhibit considerable diversity, and patrol image backgrounds vary significantly across seasons, weather, shooting time, and angles. Existing models lack universal applicability for target detection amidst varying background images [6]. 3) The real-time performance of model detection remains suboptimal. The images of UAVs and robots with cameras must be transmitted to a centralized server for analysis. The operator on duty takes corresponding operation and maintenance measures according to the identification results. Communication resources and edge computing capabilities are not fully utilized, which cannot meet real-time requirements [7]. Consequently, training DL models with high accuracy and robust generalization capabilities in environments characterized by imbalanced samples remains a formidable challenge for intelligent image recognition in the inspection of transmission equipment. Moreover, effectively integrating edge computing with DL models has emerged as a significant research focus within the realm of power Internet of Things technology.

In summary, this work delves into the construction and enhancement methods of DL-based target detection models predicated on typical defect detection scenarios in the electricity transmission line. Besides, given the aforementioned challenges, optimization efforts are undertaken across various dimensions including model input, image samples, feature extraction networks, feature fusion networks, and model output. The overarching objective is to improve the target detection model's accuracy, speed, and generalization ability, thus facilitating power grid inspectors in evaluating the condition of electricity transmission lines.

To address the above challenges, CV technology is introduced, and an improved lightweight network model is proposed for electricity transmission line defect identification, aiming to provide an efficient identification model. In this work, image enhancement and sharpening techniques are used to improve the YOLOv4-based network model through the Depth Separable Convolution (DSC) algorithm, and the lightweight network model is optimized using MobileNetV1. Among them, it is a type of convolution operation, where the convolution process is divided into two steps: Depthwise Convolution (DC) and Pointwise Convolution (PC). In the DC stage, each input channel is convolved with the corresponding convolution kernel, which can extract the feature information of each channel without increasing the number of model parameters. The purpose of this step is to capture the details of the input image by applying spatial filtering to each channel. Through experimental verification on the large-scale public dataset ImageNet, this work demonstrates the model's innovative performance in insulator defect detection, which achieves high precision detection and successfully improves the detection speed. At the same time, the ability of the model to detect insulator defects is also enhanced after the image sharpening. These innovations highlight this work's unique contribution to improving the efficiency and accuracy of predictions, affording viable and innovative solutions to the defect identification problems of electricity transmission lines in real-world applications.

2. Literature review

With the continuous advancement of the graphic processing unit (GPU) hardware, CV technology is increasingly being applied in insulator detection. Insulator images can be captured by UAVs or cameras to obtain an image set [8]. Machine learning (ML) algorithms can be applied to achieve insulator localization and insulator defect fault detection in electricity transmission lines [9]. The current research methods for insulator detection can be classified into three categories: traditional image processing, ML, and DL detection algorithms [10,11].

The traditional image processing method used for insulator detection on electricity transmission lines usually divides the insulator from the complex background by the features of image color and gray level and realizes the defect detection by algorithms. Envelope et al. (2021) improved the traditional active contour model's segmentation method through spatial distribution features and applied it to insulator detection [12]. Mei et al. (2021) used the OTSU algorithm and ant colony algorithm to segment and extract insulators in the image and determined the location of insulator defects by measuring the distance between adjacent insulators [13]. Khalil et al. (2022) proposed a detection method based on automatic vision, highlighting the crucial role of emerging technologies and methods in power system maintenance and reliability. This research combined UAV images, automatic vision technology, and an improved DL model to provide innovative solutions for the accurate positioning, detection, and maintenance of electricity transmission line insulators and related equipment, thus improving the reliability and safety of the power system [14]. With the gradual popularization of artificial intelligence, using the ML method for insulator detection become a trend. Qiu et al. (2022) adopted the DL model of improved lightweight YOLOv4 and used it to detect insulator defects. The results showed that this method could achieve high accuracy, recall, and F1 score in insulator defect detection. This research was of great significance for the reliability and security of power systems and

provided valuable research and application references for related fields [15]. Jiang et al. (2022) opted for optimized texture features to project insulator images and searched for insulator position information through the projected images [16]. Liu et al. (2021) applied the Harris corner detection algorithm to both the target image and the template image, matching feature information with template feature information. However, images were sensitive to scale changes and prone to erroneous matches, making it difficult to detect insulators in complex backgrounds [17]. The rapid development of GPU hardware technology significantly shortened the computation time of DL, realizing the application of DL technology in 3D object detection. Peng et al. (2021) utilized a pre-trained neural network model to extract external features of insulators, followed by superpixel segmentation and region detection operations to construct the output layer, ultimately achieving insulator defect detection [18]. Deng et al. (2022) employed the Single Shot MultiBox Detector (SSD) algorithm as the main framework for feature detection, conducting feature detection in two stages. Initially, the model was applied to preliminary feature extraction. Then, the model was adjusted using images with different backgrounds and interferences. This approach markedly promoted the efficiency of insulator detection [19]. Yi et al. (2022) proposed an intelligent insulator detection method based on convolutional neural networks. Insulator positioning was conducted first, followed by continuous comparison of insulators in various images within the network and detection of insulator defect features, thereby achieving insulator fault detection in complex backgrounds [20]. Wang et al. (2020) constructed an edge intelligence-based overhead transmission line icing monitoring system, proposing a lightweight visual recognition method based on discriminative-driven channel pruning for icing monitoring terminals with limited computing resources. Experimental results demonstrated that this method achieved an accuracy of 74.5 % in icing image recognition under extreme weather conditions, with a small model size suitable for resource-constrained monitoring terminals [21]. Feng et al. (2023) addressed the challenges of risk management in power system operations and proposed a method for identifying critical links in power operations based on spatiotemporal hybrid convolutional neural networks. Experimental results showed that this method could accurately identify various types of power operation links and their start and end times, with good real-time performance. The average accuracy was as high as 87.8 %, with a frame rate of 61 frames per second, which was of great significance for improving the control methods of power safety operation [22].

In summary, traditional image processing detection methods mainly rely on color and texture information as feature values. However, when there are pole towers and wire poles with similar colors in the background of insulator strings, the accuracy of the algorithm's identification decreases. Additionally, ML primarily detects the positions of target objects by selecting appropriate feature values and constructing recognition models, but this method often requires extensive computation and the computation process is quite cumbersome. In contrast, DL detection belongs to the category of supervised learning and can ignore the interference of complex backgrounds in images. This makes DL technology highly suitable for fault detection through aerial photos of insulators. Nevertheless, there are many target objects and excessively large image sizes in the images, directly affecting the efficiency of neural networks. These requirements for image analysis further increase the difficulty of intelligent insulator fault detection. The innovation of this work lies in the introduction of CV technology, applying improved lightweight network models to insulator defect identification in electricity transmission line insulators. Model performance is enhanced through image enhancement and sharpening techniques, and optimization is carried out based on the YOLOv4 network and MobileNetV1. Experimental results demonstrate that the model exhibits high accuracy in insulator defect detection, while improving detection speed without sacrificing accuracy, showcasing its ability to achieve a balance between model efficiency and accuracy. Compared to other methods, this work focuses more on capturing detailed features and meeting practical application requirements through optimization of lightweight network models. Therefore, compared to previous research, this work concentrates on the combination of efficiency and accuracy, demonstrating more innovation and practical exploration value in handling insulator defects.

3. Theoretical basis and model establishment

3.1. Image dataset and preprocessing of electricity transmission line insulators

3.1.1. GraphCut segmentation-based image augmentation

Images acquired during transmission equipment inspections frequently exhibit substantial variations in shooting angles, uneven illumination, and intricate backgrounds. To expand the image samples used for DL, the GraphCut segmentation algorithm is adopted to extract defective insulator targets. These targets are fused with the background images from real-world environments surrounding electricity transmission lines, which can generate a new composite image of defective insulators, expanding the samples [23].

The GraphCut segmentation algorithm applies the energy function $E(x)$ to decide whether each pixel in the image is a foreground or background [24]. An image is set as $G=(X, Y)$. X indicates all of the pixel nodes in the image. Y refers to the connecting edges between the nodes. For any node i, if it is a foreground target, $x_i = 1$. If it is a background, $x_i = 0$. The energy function of image segmentation is shown in equation (1):

$$\boldsymbol{E}(\boldsymbol{x}) = \sum_{i \in \boldsymbol{X}} \boldsymbol{E_1}(\boldsymbol{X}_i) + \boldsymbol{\lambda} \sum_{ij \in \boldsymbol{Y}} \boldsymbol{E_2}(\boldsymbol{x}_i, \boldsymbol{x}_j) \tag{1}$$

$\boldsymbol{E_1}$ represents the energy consumed when determining whether node i is foreground or background; $\boldsymbol{E_2}$ indicates the energy consumed when two adjacent nodes are different; λ refers to the energy balance parameter, usually set as 50. This experience has shown that this value can produce better results in many image segmentation problems. Empirical observations indicate that this particular value often yields superior outcomes by striking a balance between node weighting and energy smoothing performance. Hence, the algorithm can consider the pixel's characteristics and the relationship between neighboring pixels. Then, the maximum flow algorithm is employed

to obtain the minimum value of $\boldsymbol{E}(\boldsymbol{x})$, achieving the segmentation of insulators in the image. Subsequently, merging the segmented insulator targets with real background images of electricity transmission lines is a crucial step in generating new defective insulator image samples. The maximum flow algorithm is a graph theory algorithm used to find the maximum flow path from a source node to a sink node in a network. In this problem, each edge has a weight representing its maximum capacity flow. The maximum flow algorithm aims to find the maximum flow path through the network and can help solve various application problems, such as network flow optimization and task scheduling. Typical maximum flow algorithms include the Ford-Fulkerson and the Edmonds-Karp algorithms. Fig. 1a and b dispaly a segmentation diagram.

3.1.2. Laplacian sharpening

The complexity of the background surrounding electricity transmission lines can often result in insulator targets exhibiting colors closely resembling those of the background. It may be less distinguishable from the background on edge and overall. The Laplacian sharpening method is used for image augmentation to address this issue. Its purpose is to emphasize the target's edge details in the image and enhance the contrast. The Laplace transform of the binary insulator image $\boldsymbol{f}(\boldsymbol{x},\boldsymbol{y})$ is as follows.

$$\nabla^2 \boldsymbol{f}(\boldsymbol{x},\boldsymbol{y}) = \frac{\partial^2 \boldsymbol{f}}{\partial \boldsymbol{x}^2} + \frac{\partial^2 \boldsymbol{f}}{\partial \boldsymbol{y}^2} \tag{2}$$

The calculation of the second-order partial differentiation of binary image $\boldsymbol{f}(\boldsymbol{x},\boldsymbol{y})$ in the $\boldsymbol{x},\boldsymbol{y}$ directions is shown in equations (3) and (4):

$$\frac{\partial^2 \boldsymbol{f}}{\partial \boldsymbol{x}^2} = \boldsymbol{f}(\boldsymbol{x}+\boldsymbol{1},\boldsymbol{y}) + \boldsymbol{f}(\boldsymbol{x}-\boldsymbol{1},\boldsymbol{y}) - \boldsymbol{2f}(\boldsymbol{x},\boldsymbol{y}) \tag{3}$$

$$\frac{\partial^2 \boldsymbol{f}}{\partial \boldsymbol{x}^2} = \boldsymbol{f}(\boldsymbol{x},\boldsymbol{y}+\boldsymbol{1}) + \boldsymbol{f}(\boldsymbol{x},\boldsymbol{y}-\boldsymbol{1}) - \boldsymbol{2f}(\boldsymbol{x},\boldsymbol{y}) \tag{4}$$

It is essential to substitute equations (3) and (4) into equation (2), and the Laplace operator is:

$$\nabla^2 \boldsymbol{f}(\boldsymbol{x},\boldsymbol{y}) = \boldsymbol{f}(\boldsymbol{x}+\boldsymbol{1},\boldsymbol{y}) + \boldsymbol{f}(\boldsymbol{x}-\boldsymbol{1},\boldsymbol{y}) + \boldsymbol{f}(\boldsymbol{x},\boldsymbol{y}+\boldsymbol{1}) + \boldsymbol{f}(\boldsymbol{x},\boldsymbol{y}-\boldsymbol{1}) - \boldsymbol{4f}(\boldsymbol{x},\boldsymbol{y}) \tag{5}$$

In equation (5), the sharpening filter is [0, 1, 0; 1, −4, 1; 0, 1, 0]. This filter is applied using artwork master for convolution operation. Then, a Laplace image can be extracted. Next, by overlaying the artwork master with the Laplace image according to equation (6), the sharpened insulator image $\boldsymbol{g}(\boldsymbol{x},\boldsymbol{y})$ can be obtained. Here, the artwork master represents the reference image, which is typically used as a comparison or reference point in image processing, CV, or experiments. The reference image can be a standard image used to evaluate the performance or effectiveness of algorithms, or it can be a reference image used as input data for comparison or manipulation with other images. In image processing, the reference image is often used as a template or reference to aid in the analysis, enhancement, or modification of other images. In experimental design, the reference image is typically used for calibration of measurements, detection of changes, or validation of results. By comparing with the reference image, variations or effects in the image processing process can be better understood.

$$\boldsymbol{g}(\boldsymbol{x},\boldsymbol{y}) = \boldsymbol{f}(\boldsymbol{x},\boldsymbol{y}) - \nabla^2 \boldsymbol{f}(\boldsymbol{x},\boldsymbol{y}) \tag{6}$$

Fig. 2a and b shows the comparison of the effects before and after sharpening.

Fig. 2 suggests that the sharpened image can improve global and local contrast with high efficiency and can slightly decrease the impact of image blur and atomization [25].

3.1.3. Insulator image dataset for electricity transmission lines

Insulator images used here are partially obtained from the China power line insulator dataset published online. This dataset involves 600 normal insulator images and 248 defective insulator images. Additionally, 216 images are extracted from aerial photographs captured during UAV patrols. Other images are derived from image augmentation based on GraphCut segmentation. This augmentation process generates virtual insulator images, which, along with real insulator images from both the public dataset and

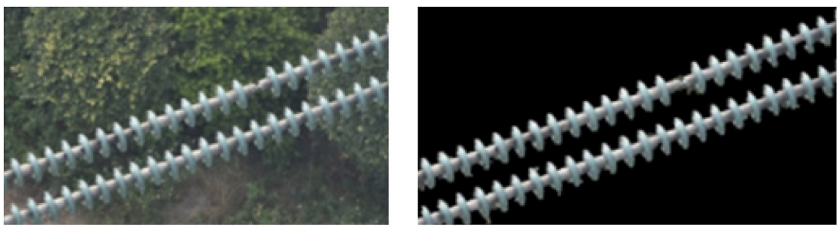

Fig. 1. A schematic diagram of image augmentation (a) Original image; (b) Segmented image.

Fig. 2. Schematic diagram of Laplacian sharpening effect (a) Image before sharpening; (b) Sharpened image.

UAV patrol inspections, collectively form the training, validation, and testing sets for examples of defective insulator detection. In total, the dataset comprises 2403 images.

Moreover, for effective training of the target detection model, the image data necessitates labeling. To this end, the MRLabeler software is employed to annotate insulators with their respective categories, locations, and identified defects. Both normal and defective insulators are labeled with the overarching category "insulator," encompassing the entire string of insulators. For defective insulators, the specific location and category of the identified defect are labeled as such, designated under the category "defect". This labeling method allows the model to learn the spatial relationship between insulators and their defects. The labeling format adopts the Pascal VOC format commonly used in the CV field.

3.2. Defect detection for electricity transmission line insulators based on improved YOLOv4

Aerial transmission equipment inspection images have problems such as too small insulator defect targets, some less significant insulators in the real environment, severe insulator overlap and occlusion, and too slow detection speed. Here, an improved YOLOv4 algorithm is proposed to rapidly and accurately detect insulator defects. Fig. 3 indicates the detection process [26].

3.2.1. DSC

DSC is the key content of Mobile Nets, and its principle is to split the 3 × 3 Standard Convolution (SC) into DW and 1 × 1 PW. The essence of DW is to use a single convolution kernel for each input channel's convolution to achieve feature information extraction. 1 × 1 PW is adopted for the linear fusion of multiple feature mAPs outputted from DW [27,28]. DSC disconnects the output channel from the convolutional kernel, reducing the model's computational complexity. Fig. 4 presents its principle compared to SC.

Assuming the size of the input image is $\boldsymbol{D_F} \times \boldsymbol{D_F} \times \boldsymbol{M}$, the calculation for the image is shown in equation (7):

$$\mathbf{C} = \boldsymbol{D_K} \bullet \boldsymbol{D_K} \bullet \boldsymbol{M} \bullet \boldsymbol{N} \bullet \boldsymbol{D_F} \bullet \boldsymbol{D_F} \tag{7}$$

$\boldsymbol{D_K}$ refers to the convolution kernel size; M and N represent the channel quantity for the input and output features, respectively. If DSC is used, the calculation of DW and PW reads:

$$\begin{cases} \boldsymbol{C_{DW}} = \boldsymbol{D_K} \bullet \boldsymbol{D_K} \bullet \boldsymbol{M} \bullet \boldsymbol{D_F} \bullet \boldsymbol{D_F} \\ \boldsymbol{C_{PW}} = \boldsymbol{M} \bullet \boldsymbol{N} \bullet \boldsymbol{D_F} \bullet \boldsymbol{D_F} \end{cases} \tag{8}$$

$\boldsymbol{C_{DW}}$ and $\boldsymbol{C_{PW}}$ are the calculation amounts corresponding to DW and PW, respectively. According to equation (8), the computational

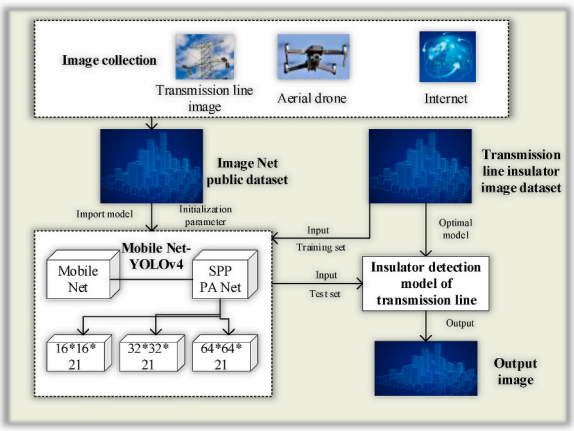

Fig. 3. Overall process of insulator defect detection for electricity transmission lines.

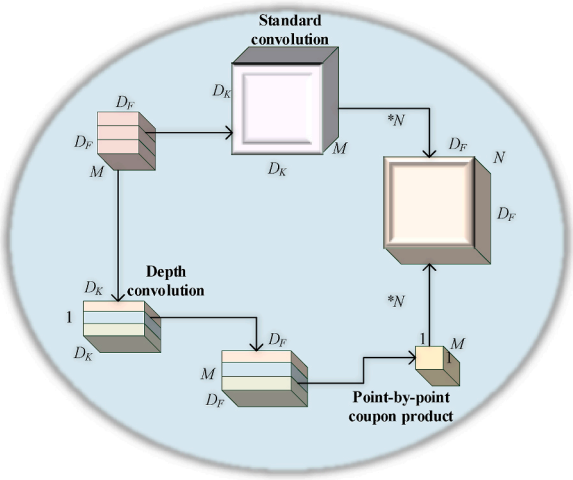

Fig. 4. Schematic diagram of DSC.

complexity of DSC is $1/N+1/D_K^2$ of the calculation amount of SC. In the general model, $N \gg D_K^2$. In Mobile Nets, the commonly used convolution kernel $D_K \times D_K$ is 3 × 3. Therefore, the computational burden of DSC is reduced to approximately 1/8–1/9 of the SC computational load, and the expression of the image is modified as equation (9):

$$\frac{D_K \bullet D_K \bullet M \bullet D_F \bullet D_F + M \bullet N \bullet D_F \bullet D_F}{D_K \bullet D_K \bullet M \bullet N \bullet D_F \bullet D_F} = \frac{1}{N} + \frac{1}{D_K^2} \tag{9}$$

Due to the high requirements for model parameters and detection speed when deployed in mobile devices, Mobile Net introduces a hyperparameter termed the width multiplier, denoted as α. This width multiplier serves to adjust the model's channel quantity, thereby impacting both its computational complexity and parameter count. Although no definitive method exists for determining the value of α, its function is to regulate model complexity by scaling the original number of channels by α. However, hyperparameter search algorithms or automated ML techniques can find the most suitable α value for specific needs while balancing performance and computational efficiency. After changing the number of channels in the model by α, the calculation for model computation is shown in equation (10):

$$C = D_K \bullet D_K \bullet \alpha M \bullet D_F \bullet D_F + \alpha M \bullet \alpha N \bullet D_F \bullet D_F \tag{10}$$

The default value of α for standard Mobile Net is 1.0. Reducing α can effectively reduce the calculation and parameter amount of the model. The value of α is typically 1.0, 0.75, 0.5, or 0.25.

3.2.2. *Improved YOLOv4 detection model*

Fig. 5 displays an improved YOLOv4 model structure based on Mobile Net V1.

In Fig. 5, the numerical annotation following DSC denotes the quantity of DSC modules employed. The Convolution Batchnormalization Relu (CBR) module is just like the Conv Batchnorm Mish (CBM) module in the YOLOv4 model, albeit substituting Mish in the

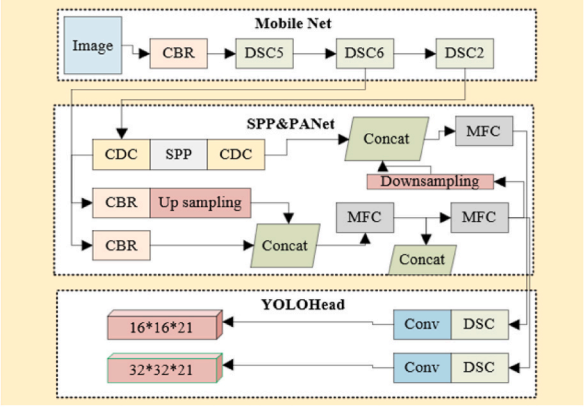

Fig. 5. Structure of the improved YOLOv4 model.

activation function layer with ReLU6. The Central Difference Convolutional (CDC) module represents that the input undergoes three convolution calculations, involving 2 convolution types: CBR and DSC. The Model of Five Convolution (MFC) module reveals that the input has undergone five convolution calculations, integrating two convolution types: CBR and DSC. Compared with YOLOv4, the improved YOLOv4 model replaces the backbone feature extraction network with Mobile Net. It introduces DSC into the feature fusion network to form DSC-Spatial Pyramid Pooling (SPP) and DSC-Path Aggregation Network (PANet).

3.2.2.1. Feature extraction network. Mobile Net serves as a novel feature extractor, supplanting the Cross Stage Partial Darknet 53 (CSPDarknet53) backbone feature extraction network in YOLOv4. Additionally, the required 224 × 224 for the initial input size of the network is normalized back to 416 × 416 [29]. According to the network structure and principle, features after 5, 6, and 2 DSC convolution modules are extracted as features 1, 2, and 3, respectively. Compared to the three feature mao scales of 52 × 52, 26 × 26, and 13 × 13 in YOLOv4, the three feature mAP sizes of the improved YOLOv4 model become 64 × 64, 32 × 32, and 16 × 16. Then, features 1, 2, and 3 are input into SPP and PANet for fusion enhancement. In addition, the activation function is replaced with the ReLU6 activation function configured for the mobile network, and its characteristic expression is shown in equation (11):

$$\boldsymbol{y} = \boldsymbol{min}\,[6, \boldsymbol{max}(\boldsymbol{x}, \boldsymbol{0})] \tag{11}$$

3.2.2.2. DSC-SPP and DSC-PANet. The test results show that the total parameter amount of YOLOv4 is approximately 64.43 million. If only the standard Mobile Net with $\alpha = 1$ is adopted to replace the CSPDarknet53 feature extraction network, the model's parameter count hovers around 41 million. The parameter quantity has not greatly decreased [30]. This is because most of the parameters in YOLOv4 are located in the SC of SPP and PANet. DSC is brought into SPP and PANet to achieve further model lightweight and optimized into DSC-SPP and DSC-PANet. The specific details are as follows. The first step is to replace the SC module comprised of 3 CBRs before and after the SPP network with a CDC module. It means that the second CBR in Conv × 3 is replaced with DSC, while maintaining the number of output channels unchanged. The second step is to improve the five SC (Conv × 5) modules in the PANet to MFC modules, replacing the second and fourth CBRs with DSC. The third step is to replace the SC with a kernel of 3 × 3 in YOLOHead with DSC [31]. Upon implementing these modifications, the total parameter count of the improved YOLOv4 detection model

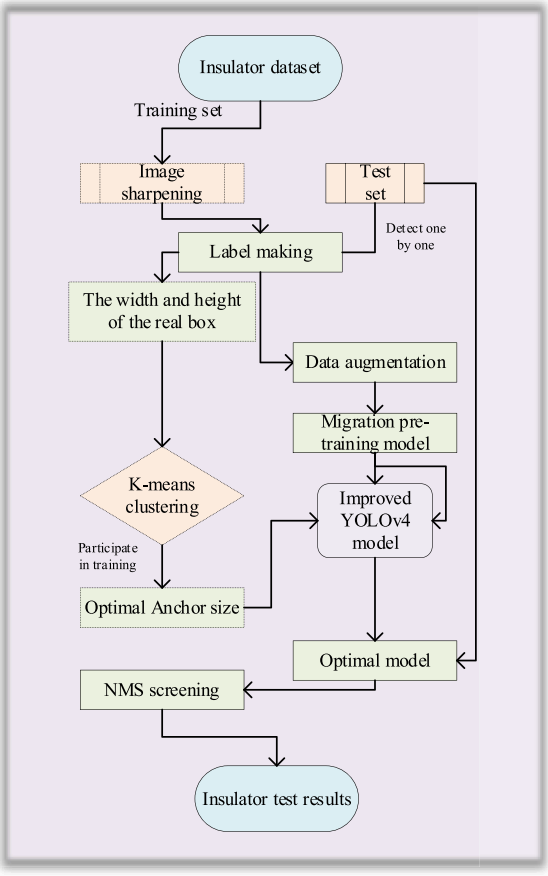

Fig. 6. Model training and testing process.

approximates 12.75 million, significantly reducing its footprint compared to the original YOLOv4 model [32].

3.3. Experimental design

3.3.1. Experimental process and parameter settings

The model undergoes training and testing procedures as outlined in Fig. 6. Moreover, ImageNet, a large public dataset, is used for model pre-training. It is migrated to the insulator image dataset of the electricity transmission line through a staged transfer learning method. Before model training, geometric and optical transformations, involving flipping, scaling, and hue, are randomly adopted to expand the sample. In addition, training techniques such as label smoothing, Mosaic data enhancement, and cosine annealing attenuation are integrated to fortify the model's robustness and generalization ability.

The primary frame sizes delineated in Fig. 6 are derived via clustering on the training set utilizing the K-means clustering algorithm. Its sizes manifest as [15 14, 21 135, 21 15; 39 18, 81 21, 107 36; 252 52, 265 80, 266 126], representing nine sets of prior frames with varying dimensions. The prior frames within the first, middle, and last three size groups correspond to feature mAPs at resolutions of 16 × 16, 32 × 32, and 64 × 64, respectively. They are used for the detection of targets of different sizes. Table 1 illustrates the parameter settings during the training and testing of the improved YOLOv4 model.

4. Experimental results and analysis

4.1. Effects of different indicators on the effectiveness of detection models

4.1.1. Impact of various sample ratios

To assess the impact of sample size on the detection accuracy of the improved YOLOv4 model, the ratio of image samples in the training set (including the validation set) to those in the test set is systematically adjusted to 5:5, 6:4, 7:3, 8:2, and 9:1, respectively. Moreover, 10 % of the image samples in the training set are taken as a verification set. Table 2 exhibits the specific sample distribution. Table 3 outlines test results under different sample ratios, encompassing P-value, R-value, Average Precision (AP), and mAP performance indicators.

Tables 2 and 3 reveal an upward trend in P, R, AP, and mAP values as the ratio of training sets to test sets increases. Among them, AP-Insulator, P-Insulator, and mAP are key metrics employed to evaluate the performance of object detection models, especially crucial when dealing with specific categories such as insulators. AP-Insulator measures the model's AP in detecting insulators, reflecting the model's stability and accuracy in identifying insulators. P-Insulator focuses more on the proportion of true insulators detected by the model, indicating its precision. Meanwhile, mc is a comprehensive performance indicator for multi-class object detection tasks, evaluating the model's overall performance by calculating the mean of all class APs. A higher mAP suggests a more balanced and outstanding detection capability across different categories. These metrics are of significant importance in applications such as power systems, not only helping to understand the model's performance in detecting critical equipment like insulators but also offering essential insights for optimizing and improving the model. By continually enhancing these metrics, the accuracy and reliability of object detection models can be improved, thus better safeguarding the safe and stable operation of power systems. Furthermore, the impact on defect targets is greater, and the upward trend is more significant. When the sample ratio is set to 9:1, the number of training and validation samples is sufficient, and almost all performance indicators in the model test results can reach the maximum value, with each indicator over 90 %, and the mAP value reaching 93.8 %. The model achieves the highest detection accuracy at this time. Hence, the 9:1 sample allocation ratio is used in subsequent analyses of different width multipliers α, detection, and sharpening algorithms.

4.1.2. Test results for different width multipliers α

Simulation tests are conducted for common values of α, such as 0.25, 0.50, 0.75, and 1.0, and their results are compared and analyzed to analyze the impact of α on detection accuracy. Table 4 lists the test results' P-value, R-value, AP, and mAP indicators under various α values.

Table 4 elucidates that as the α value increases, the P, R, and AP values of defective insulators show an upward trend. The values of R and AP of normal insulators exhibit an upward trend, while the P value mildly decreases, but both are over 94 %. Moreover, the overall mAP of normal insulators showcases a similar upward trend. The other performance indicators attain their peak values when α = 1.0, except for the P value of the normal insulator class. According to the actual application deployment, the α value can be flexibly adjusted to achieve lightweight, high accuracy, and high real-time performance of the model.

Table 1
Parameter configuration of improved YOLOv4 model.

Parameter name	Stage 1	Stage 2
Batch size	8	2
Initial learning rate	$1*10^{-3}$	$1*10^{-4}$
Training times	50	50
Non-Maximum Suppression (NMS) threshold	0.3	
Sample proportion	9:1	
Label smoothing value	0.01	
The minimum learning rate of cosine annealing	$1*10^{-6}$	

Table 2
Distribution of diverse sample ratios.

The proportion of the number of image samples		5:5	6:4	7:3	8:2	9:1
Name of datasets	Training set	1081	1297	1514	1730	1946
	Verification set	120	144	168	192	216
	Test set	1202	962	721	481	241

Table 3
Test results for different sample ratios.

Names of index		AP-insulator (%)	P-insulator (%)	R-insulator (%)	mAP (%)	AP-defect (%)	P-defect (%)	R-defect (%)
The proportion of the number of image samples	5:5	90.2	95.1	81	86	82.5	91	77.8
	6:4	92.5	95	85	90	87.5	91.5	84
	7:3	92.6	95.4	84	89	87	94	85.5
	8:2	90.3	94	83	88.5	88	91	85
	9:1	94.5	95	91	93.8	92	97.5	93

Table 4
Test results of different width multipliers α

Names of index		AP-insulator (%)	P-insulator (%)	R-insulator (%)	mAP (%)	AP-defect (%)	P-defect (%)	R-defect (%)
Width multiplierα	0.25	85	97	72.5	71	60	75	48
	0.5	91	95	85	87	84	79	84
	0.75	95	96	90	90	91	93	91
	1	94	95	89	91	92	95	92

4.1.3. Impact of different sharpening algorithms

To mitigate challenges related to indistinct contours and low contrast resulting from the similarity between insulators and the background environment, a Laplacian sharpening method is employed to enhance the insulator target contours. Moreover, a comparison is made between this method and the other three sharpening methods, namely the Sobel, Prewitt, and Laplace operators. Table 5 depicts the detection result of the model after image processing using different sharpening methods.

Table 5 underscores that the AP value of the insulator defect class is higher when employing the image sharpening method compared to non-sharpening processing. It can be understood as improving the model's detection ability for insulator defects after introducing image sharpening processing. Among the four sharpening algorithms considered, Laplacian sharpening emerges as the optimal performer across all insulator indicators, boasting the highest AP and R values for insulator defects. Furthermore, the overall mAP achieved by this method can reach an impressive 97.3 %, highlighting its capacity for attaining the highest detection accuracy.

4.2. Comparison of effects of various detection models

In addition to the improved YOLOv4 model, four models of Fast Region-based Convolutional Neural Network (RCNN), SSD, YOLOv3, and YOLOv4 are implemented for comparison. Table 6 presents the detection results of various algorithms under the same training and test sets. The α value of Mobile Net in the improved YOLOv4 model is 1.0.

Table 6 portrays that among all defect detection models, YOLOv4, EfficientDet, improved YOLOv4, and CenterNet show superior performance in terms of insulator detection capability. Notably, these models exhibit commendable AP-insulator (%) scores, with values reaching 96.0, 91.2, 94.5, and 93.4, respectively. Similarly, their F1 score-insulator scores reflect high levels of performance, with scores standing at 96.0, 90.5, 95.9, and 92.7, respectively. It is worth noting that the improved YOLOv4 has achieved excellent performance in all aspects. Its AP scores in the insulator and defect categories (94.5 and 93.1, respectively) demonstrate its superiority in overall performance. In addition, its high FPS value of 53 further highlights its efficient performance in real-time scenarios. The comparison matrix between the improved model and the defect model is listed in Table 7.

In Table 7, the improved model exhibits higher precision and recall in defect detection tasks. There are 480 defects accurately

Table 5
Test results of different sharpening methods.

Names of index		AP-insulator (%)	P-insulator (%)	R-insulator (%)	mAP (%)	AP-defect (%)	P-defect (%)	R-defect (%)
Sharpening method	No sharpening	94.5	96	91.6	93.8	93.1	97	94.1
	Prewitt	94	93.9	89.3	93.8	93.6	93.9	93.8
	Sobel	94.7	93.4	91.4	95.2	95.6	98.4	95.2
	Log	94.3	95.2	89.7	94	93.6	96.9	93.9
	Laplacian	96.1	96.7	93.9	97.3	98.4	96	97.3

Table 6
Detection result comparison of different algorithms.

Names of index		AP-insulator (%)	F1 score-insulator ($*10^{-2}$)	mAP (%)	AP-defect (%)	F1 score-defect ($*10^{-2}$)	FPS
Detection model	Faster RCNN	87.3	79	80	92.5	92	1
	SSD	93.8	81	84.4	75	72	28
	YOLOv1	81	75	81.2	82.3	83	17
	YOLOv2	84.2	83	85	84	85	20
	YOLOv3	89	88	88.2	87	89	24
	YOLOv4	96	96	96.2	96.4	95	19
	EfficientDet	91.2	90.5	89.7	88.6	87.8	35
	RetinaNet	88.7	87.2	86.4	90.2	89.5	30
	CenterNet	93.4	92.7	91.8	85.6	84.2	40
	Cascade R–CNN	94.8	94.2	93.6	88.9	87.5	15
	HRNet	90.1	89.4	88.7	91.5	90.9	25
	Improved YOLOv4	94.5	95.9	93.8	93.1	94	53

identified as defects (True Positive). However, 20 defects are mistakenly classified as normal (False Negative), representing a certain level of omission. Additionally, 15 normals are wrongly predicted as defects (False Positive), and 385 normals are correctly classified as normal (True Negative). The model demonstrates high accuracy in defect detection, but further improvement is needed for the omission rate. Overall, the improved model may achieve good results in practice, but continuous refinement is still necessary to enhance overall performance levels. Overall, different models show their advantages in various tasks and categories. The improved YOLOv4 model's comprehensive performance and real-time processing speed make it the first choice worthy of attention, while the performance of other models in diverse categories and indicators needs to be comprehensively weighed and selected according to actual needs.

5. Discussion

This work has made prominent contributions in the CV field, particularly in the application of object detection algorithms. Addressing the issue of insulator defect detection in electricity transmission lines, a series of innovative methods and strategies are proposed, achieving efficient and precise detection of insulator defects. Firstly, this work delves into the construction, augmentation, and preprocessing of insulator defect image datasets. To address potential sample imbalance issues in practical applications, this work proposes a data augmentation method based on GraphCut segmentation, effectively expanding the quantity and diversity of defective insulator images. This not only provides rich data support for subsequent model training but also enhances the model's generalization ability. Secondly, this work focuses on lightweight improvements to the YOLOv4 algorithm to reduce model complexity, decrease memory consumption, and improve detection speed. By adopting MobileNet as the feature extraction network and combining DSC-SPP and DSC-PANet structures, a highly efficient and lightweight insulator defect detection model is successfully constructed. While maintaining high detection accuracy, this model significantly advances detection speed, meeting the requirements of real-time edge detection devices. Additionally, this work employs Laplacian sharpening preprocessing technology to enhance image details and edge sharpness, further improving the model's detection performance. Through this method, potential shortcomings in detection accuracy of the lightweight YOLOv4 model are successfully addressed, achieving an overall detection accuracy level of 97.3 %. In summary, this work has made significant contributions to insulator defect detection in electricity transmission lines. By optimizing datasets, improving algorithm structures, and introducing new preprocessing techniques, an efficient and accurate insulator defect detection model is successfully implemented. This work can offer strong support for safety inspections in the power industry and provide valuable insights for the application of CV technology in other fields. Compared to the study by Gai et al. (2023) [33], this work enhances the accuracy and speed of the electricity transmission line defect identification model by introducing CV technology. The use of advanced techniques such as DSC optimizes the model, demonstrating excellent performance in experiments. By constructing a comprehensive insulator image dataset and discussing the impact of different parameters on model effectiveness, the model's optimal parameter configuration is revealed. Compared to other algorithms, the model exhibits unique advantages in detection efficiency and accuracy, providing an innovative and feasible solution for electricity transmission line defect detection.

6. Conclusion

This work aims to enhance the accuracy, speed, and generalization capability of object detection models to assist grid inspectors in detecting the status of electricity transmission lines. Firstly, a GraphCut-based segmentation algorithm is employed to expand the sample of defective insulator images, and the Laplacian algorithm is used to sharpen the image set, thereby constructing a comprehensive insulator image dataset of electricity transmission lines. Secondly, on account of MobileNet V1, DSC-SPP, and DSC-PANet, improvements to the insulator defect detection model are achieved on the basis of YOLOv4. Additionally, the effects of different sample ratios, width multiplier α, and sharpening methods on the model's detection results are discussed. The detection results of the improved YOLOv4 model are compared with other object detection algorithms (such as Faster RCNN, SSD, YOLOv3, and YOLOv4). The results indicate that when the sample ratio is set to 9:1, there is sufficient training and validation sample quantity. Almost all performance indicators in the model's detection results can reach their maximum values, with each indicator exceeding 90 %, and the

Table 7
The comparison matrix between the improved model and the defect model.

Actual/Forecast	Improved	Defect
Improved	TP = 480	FN = 20
Defect	FP = 15	TN = 385

mAP value reaching 93.8 %. This suggests that the model achieves the highest detection accuracy in this setting. At $\alpha = 1.0$, all other performance indicators reach their maximum values, except for the P value of the normal insulator category. Compared to without sharpening processing, using image sharpening methods results in higher AP values for the insulator defect category. This implies that the model's ability to detect insulator defects is improved after introducing image sharpening processing. The image detection speed of the improved YOLOv4 is approximately 2.8 times faster than YOLOv4, indicating that the model can detect insulator defects on electricity transmission lines with high accuracy and speed. A limitation of this work lies in the fact that the availability and accuracy of the object detection model heavily depend on the training image data, while there is a scarcity of actual aerial inspection images from grid line patrols. Particularly, electricity transmission lines contain numerous insulators with multiple defects and various foreign objects. In real patrol images, there exists a severe imbalance between normal and defective samples. Therefore, further optimization of sample quantity is necessary to effectively identify and detect defects in electricity transmission lines. This work has made significant contributions to the detection of insulator defects in electricity transmission lines. Through the optimization of datasets, improvements in the YOLOv4 algorithm structure, and the introduction of Laplacian sharpening preprocessing techniques, an efficient and accurate detection model has been successfully developed. This achievement enables real-time and precise detection of insulator defects, furnishing robust support for safety inspections in the power industry.

However, the limitations of the object detection model in actual aerial inspection images necessitate further exploration. Firstly, the training image data is added, the training set is expanded by data enhancement technology, and the defect samples and insulator foreign bodies are artificially synthesized to enhance the model's adaptability. Secondly, cross-dataset adaptation methods are introduced to improve the model's accuracy and robustness on imbalanced data by using data from other fields or sources. Additionally, the model's generalization capability is enhanced by utilizing transfer learning and multi-task learning to handle different types and complex defects in electricity transmission lines. Finally, integrating other information sources, such as sensor data and time-series data, the performance of the object detection model can be improved by comprehensively utilizing multi-source information. Simultaneously, to enhance the model's classification performance, data preprocessing and feature engineering can be optimized, suitable models and hyperparameters can be selected, and imbalanced datasets can be processed. Moreover, ensemble learning and model fusion strategies can be applied, regularization can be used to prevent overfitting, and post-processing optimization can be carried out. The comprehensive application of these measures can effectively improve classification performance.

Data availability statement

All data generated or analyzed during this study are included in this published article [and its supplementary information files]. If someone wants to request the data from this study please contact the Corresponding author (Lanhang Chen*, chenlanhang@126.com).

CRediT authorship contribution statement

Chen Lanhang: Writing – review & editing, Writing – original draft, Validation, Supervision, Resources, Methodology, Investigation, Formal analysis, Data curation, Conceptualization.

Declaration of competing interest

The authors declare that they have no known competing financial interests or personal relationships that could have appeared to influence the work reported in this paper.

Appendix A. Supplementary data

Supplementary data to this article can be found online at https://doi.org/10.1016/j.heliyon.2024.e30405.

References

[1] X. Li, Z. Li, H. Wang, W. Li, Unmanned aerial vehicle for transmission line inspection: status, standardization, and perspectives, Front. Energy Res. 9 (1) (2021) 713634.
[2] F. Nekovar, J. Faigl, M. Saska, Multi-tour set traveling salesman problem in planning power transmission line inspection, IEEE Rob. Autom. Lett. 6 (4) (2021) 6196–6203.
[3] Y. Zhang, C. Lv, D. Wang, W. Mao, J. Li, A novel image detection method for internal cracks in corn seeds in an industrial inspection line, Comput. Electron. Agric. 197 (7) (2022) 106930.

[4] M. Witek, Structural integrity of steel pipeline with clusters of corrosion defects, Materials 14 (852) (2021) 1–15.
[5] X. Hu, H. Liu, C. Qiu, D. Liu, Inspection of line defects in transition metal dichalcogenides using a microscopic hyperspectral imaging technique, J. Phys. Chem. Lett. 2022 (9) (2022) 13.
[6] F. Zhou, G. Wang, Y. Zheng, SA RCNN for occluded damper detection in the inspection of power transmission line, J. Phys. Conf. 1871 (1) (2021) 012081.
[7] Y. Ma, Q. Li, L. Chu, Y. Zhou, C. Xu, Real-time detection and spatial localization of insulators for UAV inspection based on binocular stereo vision, Rem. Sens. 13 (2) (2021) 230.
[8] S.F. Stefenon, M.P. Corso, A. Nied, F.L. Perez, Classification of insulators using neural network based on computer vision, IET Gener. Transm. Distrib. 2022 (6) (2022) 16.
[9] Z. Wan, Q.D. Wang, D. Liu, J. Liang, Effectively improving the accuracy of PBE functional in calculating the solid band gap via machine learning, Comput. Mater. Sci. 198 (18) (2021) 110699.
[10] LauraFarrelly Pilozzi, A. Francis Marcucci, Claudio GiuliaConti, Topological nanophotonics and artificial neural networks, Nanotechnology 32 (14) (2021) 4–5.
[11] C. Liu, Y. Wu, J. Liu, J. Han, MTI-YOLO: a light-weight and real-time deep neural network for insulator detection in complex aerial images, Energies 14 (5) (2021) 1426.
[12] G. Envelope, H.A. Min, Z.B. Feng, Z.A. Min, Insulator detection and damage identification based on improved lightweight YOLOv4 network - ScienceDirect, Energy Rep. 7 (5) (2021) 187–197.
[13] H. Mei, H. Jiang, F. Yin, Terahertz imaging method for composite insulator defects based on edge detection algorithm, IEEE Trans. Instrum. Meas. 2021 (70) (2021) 70.
[14] E.H. Khalil, K. Adam, M. Kelly, Towards the in-situ detection of spin charge accumulation at a metal/insulator interface using STEM-EELS technique, Microsc. Microanal. 2022 (1) (2022) 1.
[15] Z. Qiu, X. Zhu, C. Liao, D. Shi, W. Qu, Detection of transmission line insulator defects based on an improved lightweight YOLOv4 model, Appl. Sci. 12 (3) (2022) 1207.
[16] Y. Jiang, S. Li, P. Zhu, Electrochemical DNA biosensors based on the intrinsic topological insulator BiSbTeSe 2 for potential application in HIV determination, ACS Appl. Bio Mater. 5 (3) (2022) 1084–1091.
[17] C. Liu, Y. Wu, J. Liu, Improved YOLOv3 network for insulator detection in aerial images with diverse background interference, Electronics 10 (7) (2021) 771.
[18] H. Peng, Z. Wang, X. Liu, Railway insulator detection based on adaptive cascaded convolutional neural network, IEEE Access 9 (99) (2021), 1–1.
[19] F. Deng, Z. Xie, W. Mao, Research on edge intelligent recognition method oriented to transmission line insulator fault detection, Int. J. Electr. Power Energy Syst. 139 (5) (2022) 108054.
[20] L.A. Yi, B. Mn, Y. Envelope, Insulator defect detection for power grid based on light correction enhancement and YOLOv5 model, Energy Rep. 8 (8) (2022) 807–814.
[21] B. Wang, F. Ma, L. Ge, H. Ma, H. Wang, M.A. Mohamed, Icing-EdgeNet: a pruning lightweight edge intelligent method of discriminative driving channel for ice thickness of transmission lines, IEEE Trans. Instrum. Meas. 70 (2020) 1–12.
[22] L. Feng, B. Wang, F. Ma, H. Ma, M.A. Mohamed, Identification of key links in electric power operation based-spatiotemporal mixing convolution neural network, Comput. Syst. Sci. Eng. 46 (2) (2023).
[23] R. Sundaram, S.K. Vasudevan, Marker and modified graph cut algorithm for augmented reality gaming, Int. J. Adv. Intell. Paradigms 2022 (2) (2022) 22.
[24] Z. Long, Y. Gao, H. Meng, Clustering based on local density peaks and graph cut, Inf. Sci. 600 (7) (2022) 263–286.
[25] S.S. Khan, M. Khan, Y. Alharbi, Hybrid sharpening transformation approach for multifocus image fusion using medical and nonmedical images, J. Healthcare Eng. 2021 (15) (2021) 2021.
[26] K. Wang, M. Liu, Toward structural learning and enhanced YOLOv4 network for object detection in optical remote sensing images, Adv. Theory Simul. 2022 (6) (2022) 5.
[27] Y. Huang, Transfer remaining useful life estimation of bearing using depth-wise separable convolution recurrent network, Measurement 176 (1) (2021) 90–91.
[28] Z. Huang, J. Wu, F. Xie, Automatic surface defect segmentation for hot-rolled steel strip using depth-wise separable U-shape network, Mater. Lett. 301 (8) (2021) 130271.
[29] E. Alsaadi, N. Abbadi, An automated mammals detection based on SSD-mobile Net, J. Phys. Conf. 1879 (2) (2021) 022086.
[30] X. Li, C. Duan, Y. Zhi, Wafer crack detection based on Yolov4 target detection method, J. Phys. Conf. 1802 (2) (2021) 022101.
[31] F. Li, Z. Jiang, S. Zhou, Spilled load detection based on lightweight YOLOv4 trained with easily accessible synthetic dataset, Comput. Electr. Eng. 100 (8) (2022) 107944.
[32] B. Yang, J. Wang, An improved helmet detection algorithm based on YOLO V4, Int. J. Found. Comput. Sci. 33 (7) (2022) 887–902.
[33] R. Gai, N. Chen, H. Yuan, A detection algorithm for cherry fruits based on the improved YOLO-v4 model, Neural Comput. Appl. 35 (19) (2023) 13895–13906.